Received: 17 December 2022 | Revised: 16 February 2023 | Accepted: 21 February 2023

DOI: 10.1111/mmi.15048

RESEARCH ARTICLE

WILEY

The Mba1 homologue of *Trypanosoma brucei* is involved in the biogenesis of oxidative phosphorylation complexes

Christoph Wenger[1] | Anke Harsman[1] | Moritz Niemann[1] | Silke Oeljeklaus[2] | Corinne von Känel[1] | Salvatore Calderaro[1] | Bettina Warscheid[2,3] | André Schneider[1,4]

[1]Department of Chemistry, Biochemistry and Pharmaceutical Sciences, University of Bern, Bern, Switzerland

[2]Faculty of Chemistry and Pharmacy, Biochemistry II, Theodor Boveri-Institute, University of Würzburg, Würzburg, Germany

[3]CIBSS Centre for Integrative Biological Signalling Studies, University of Freiburg, Freiburg, Germany

[4]Institute for Advanced Study (Wissenschaftskolleg) Berlin, Berlin, Germany

Correspondence
André Schneider, Department of Chemistry, Biochemistry and Pharmaceutical Sciences, University of Bern, Freiestrasse 3, Bern, Switzerland.
Email: andre.schneider@unibe.ch

Present address
Moritz Niemann, Mattei Team, EMBL Imaging Centre, Heidelberg, Germany

Funding information
Germany's Excellence Strategy, Grant/Award Number: CIBSS - EXC-2189 - Project ID 390939984; NCCR RNA & Disease, a National Centre of Competence in Research, Grant/Award Number: 205601; Schweizerischer Nationalfonds zur Förderung der Wissenschaftlichen Forschung, Grant/Award Number: 205200

Abstract

Consistent with other eukaryotes, the *Trypanosoma brucei* mitochondrial genome encodes mainly hydrophobic core subunits of the oxidative phosphorylation system. These proteins must be co-translationally inserted into the inner mitochondrial membrane and are synthesized by the highly unique trypanosomal mitoribosomes, which have a much higher protein to RNA ratio than any other ribosome. Here, we show that the trypanosomal orthologue of the mitoribosome receptor Mba1 (TbMba1) is essential for normal growth of procyclic trypanosomes but redundant in the bloodstream form, which lacks an oxidative phosphorylation system. Proteomic analyses of TbMba1-depleted mitochondria from procyclic cells revealed reduced levels of many components of the oxidative phosphorylation system, most of which belong to the cytochrome c oxidase (Cox) complex, three subunits of which are mitochondrially encoded. However, the integrity of the mitoribosome and its interaction with the inner membrane were not affected. Pull-down experiments showed that TbMba1 forms a dynamic interaction network that includes the trypanosomal Mdm38/Letm1 orthologue and a trypanosome-specific factor that stabilizes the CoxI and CoxII mRNAs. In summary, our study suggests that the function of Mba1 in the biogenesis of membrane subunits of OXPHOS complexes is conserved among yeast, mammals and trypanosomes, which belong to two eukaryotic supergroups.

KEYWORDS
Mba1, mitochondria, mitoribosome, oxidative phosphorylation, *Trypanosoma*

1 | INTRODUCTION

Mitochondria or mitochondria-derived organelles are a defining feature of eukaryotic cells. They originated from a single endosymbiotic event between an α-proteobacterium and an archaeal host cell, 1.7–2.1 billion years ago (Betts et al., 2018; Roger et al., 2017; Spang et al., 2015; Wang & Wu, 2015; Zaremba-Niedzwiedzka et al., 2017). During the endosymbiont-to-mitochondria transition, most of the endosymbiont's genes were either lost or transferred to the genome of the host cell (Dacks et al., 2016; Roger et al., 2017). However, a small number of genes were retained in the mitochondrial DNA (mtDNA). Thus, mitochondria contain a complete transcription and translation machinery, including ribosomes termed mitoribosomes.

Many of the genes that were retained in the mtDNA are highly hydrophobic core subunits of the oxidative phosphorylation (OXPHOS) complexes (Roger et al., 2017). Thus, the mtDNA of *Saccharomyces cerevisiae* codes for eight proteins, seven of which are hydrophobic components of the OXPHOS complexes (Desai et al., 2017; Freel et al., 2015; Wolters et al., 2015). These proteins are co-translationally inserted into the inner mitochondrial membrane (IM) by the oxidase assembly protein 1 (Oxa1) (Ott & Herrmann, 2010), a homologue of the bacterial insertase YidC (McDowell et al., 2021; Scotti et al., 2000). Oxa1 has a large hydrophilic, matrix-facing C-terminal domain that was shown to be in close proximity to the mitoribosomal proteins (MRPs) uL23 and uL24 of the mitoribosomal large subunit (mt-LSU) (de Silva et al., 2015; Gruschke et al., 2010). This is in line with the fact that in *S. cerevisiae*, all mitoribosomes are associated with the IM (Ott & Herrmann, 2010).

Interestingly, mitoribosomes remain associated with the IM even in the absence of Oxa1 (Keil et al., 2012), indicating that additional factors are involved in the IM association of mitoribosomes. Indeed, several such factors have been discovered. The first one identified, termed multi-copy bypass of AFG3 or Mba1 (Rep et al., 1996; Rep & Grivell, 1996), is peripherally associated with the IM on the matrix side and serves as a mitoribosome receptor (Rep & Grivell, 1996). It is in close proximity to the MRPs uL22 and uL29 (de Silva et al., 2015; Gruschke et al., 2010) and aligns the peptide exit tunnel of the mitoribosome with the insertion site of Oxa1 at the IM (Gruschke et al., 2010; Ott et al., 2006). Mba1 interacts with the mitochondrial distribution and morphology protein 38 (Bauerschmitt et al., 2010) (Mdm38, in other organisms referred to as Letm1), an integral IM protein also involved in the association of mitoribosomes with the IM (Frazier et al., 2006). Mba1 and Mdm38 might additionally be involved in the recruitment of mRNA stabilization and translation factors (Bauerschmitt et al., 2010). Finally, the expansion segment 96-ES1 of the yeast mitochondrial 21 S rRNA has also been shown to contribute to the IM association of mitoribosomes (Pfeffer et al., 2015). An impaired co-translational IM integration leads to decreased activity of the OXPHOS complexes, since they rely on mitochondrially encoded subunits (Keil et al., 2012; Preuss et al., 2001; Rep & Grivell, 1996). Mdm38 was additionally shown to have a second role in the cell's K^+/H^+ homoeostasis (Nowikovsky et al., 2007).

Mitochondrial protein biogenesis, including co-translational IM integration of mitochondrially encoded proteins, is best understood in *S. cerevisiae* and mammals, both belonging to the eukaryotic supergroup Amorphea (Burki et al., 2020). The arguably next best understood system concerning mitochondrial protein biogenesis is the unicellular parasite *Trypanosoma brucei*. It belongs to a different eukaryotic supergroup, called the Discoba, which is essentially unrelated to the Amorphea (Burki et al., 2020). Indeed, the work on mitochondrial protein biogenesis in *T. brucei* showed that, even though the general pathways are conserved, the involved complexes are astonishingly diverse (Harsman et al., 2016; Mani et al., 2015; Schneider, 2020; Schneider, 2022).

T. brucei undergoes a complex life cycle, during which it adapts to very different environments. In the midgut of its insect vector, the Tsetse fly, the procyclic form (PCF) of *T. brucei* encounters glucose-poor and amino acid-rich conditions (Figueiredo et al., 2017). Here, it uses proline as its main energy source (Lamour et al., 2005; Mantilla et al., 2017). The OXPHOS system is fully functional and the single mitochondrion of *T. brucei* forms an intricate network spanning the whole cell (Matthews, 2005; Vickerman, 1985). As in *S. cerevisiae*, most of the genes encoded on the trypanosomal mtDNA, termed kinetoplast DNA (kDNA), are subunits of the OXPHOS complexes. Twelve of the 18 protein-coding transcripts encode for subunits of the OXPHOS complexes (Clement et al., 2004; Ramrath et al., 2018; Verner et al., 2015). The bloodstream form (BSF) of *T. brucei*, found in the blood of its mammalian host, produces energy by glycolysis using glucose as an energy source (Matthews, 2005; Vickerman, 1985). Here, the mitochondrion is heavily reduced and OXPHOS complexes are absent (Matthews, 2005; Zíková et al., 2017), with the exception of the ATP synthase, which however functions in reverse in an ATP-consuming manner to maintain the membrane potential (Nolan & Voorheis, 1992; Schnaufer et al., 2005).

To date, one of the least understood processes of mitochondrial protein biogenesis in *T. brucei* is the integration of mitochondrially encoded proteins into the IM. Here, we identify the protein Tb927.7.4620 as the trypanosomal orthologue of Mba1 (TbMba1). We present data showing that TbMba1 is essential for the maturation and/or stability of trypanosomal OXPHOS complexes. Furthermore, we show that it interacts with the trypanosomal orthologue of Letm1/Mdm38 and with the trypanosome-specific Tb927.11.16250, a stabilizing factor of the mitochondrial mRNAs encoding cytochrome c oxidase subunit I (CoxI) and CoxII.

2 | RESULTS

2.1 | Tb927.7.4620 is an orthologue of yeast Mba1

A recent phylogenomic analysis identified the *Leishmania major* protein Lmjf1.14.0080 as the orthologue of yeast Mba1 (Pyrih et al., 2021). *L. major*, like *T. brucei*, is a trypanosomatid (Kaufer et al., 2017) and thus belongs to the Discoba (Burki et al., 2020). When we did BLAST searches for the orthologue of Lmjf.14.0080 in *T. brucei*, we identified Tb927.7.4620 as its homologue. Excluding the predicted N-terminal presequences (MitoProt II server: https://ihg.gsf.de/ihg/mitoprot.html), the two proteins show an identity of 62.5% and a similarity of 76.0% (Figure S1a). An alignment between Tb927.7.4620 and yeast Mba1 (Uniprot: P38300), excluding the predicted N-terminal presequences, reveals a 18.3% identity and 31.3% similarity (Figure S1b). Moreover, AlphaFold structure models show large similarities between Tb927.7.4620, yeast Mba1 and the human Mba1 orthologue mL45 (Jumper et al., 2021; Varadi et al., 2022). In summary, these findings indicate that Tb927.7.4620 is the Mba1 orthologue in *T. brucei*, which is why we termed it TbMba1.

2.2 | TbMba1 is an essential membrane-associated mitochondrial protein in PCF *T. brucei*

To functionally analyse TbMba1 a *T. brucei* PCF cell line, allowing inducible RNA interference (RNAi) against the open reading frame (ORF) of TbMba1 was established. The growth of uninduced (-Tet) and induced (+Tet) RNAi cells was analysed over 6 days. The knockdown of TbMba1 in PCF *T. brucei* led to a strong growth retardation starting after 2 days of induction, indicating that TbMba1 is essential for normal growth in this life cycle stage (Figure 1a). In contrast, in *S. cerevisiae*, depletion of Mba1 alone does not cause a growth defect (Ott et al., 2006). Interestingly, we were able to generate a double knockout (dKO) *T. brucei* BSF cell line, replacing the two alleles of TbMba1 with the antibiotic resistance cassettes of hygromycin and blasticidin respectively (Figures 1b and S2a). TbMba1 is therefore not required for normal growth of BSF *T. brucei* indicating it has a PCF-specific function. This is in line with a previous study, which showed that TbMba1 expression is 11-fold lower in BSF cells when compared to the PCF of *T. brucei* (Urbaniak et al., 2012).

In a previous proteomics study, TbMba1 was shown to be mitochondrially localized (Peikert et al., 2017). To confirm this finding, TbMba1 was C-terminally myc-tagged (TbMba1-myc) and ectopically expressed in a PCF RNAi cell line targeting the 3′-untranslated region (3′-UTR) of the endogenous TbMba1 mRNA. This results in essentially exclusive expression of TbMba1-myc. TbMba1-myc complemented the growth phenotype caused by the depletion of the endogenous TbMba1, proving that the tag does not interfere with TbMba1 function (Figure S2b,c). Next, we analysed the localization

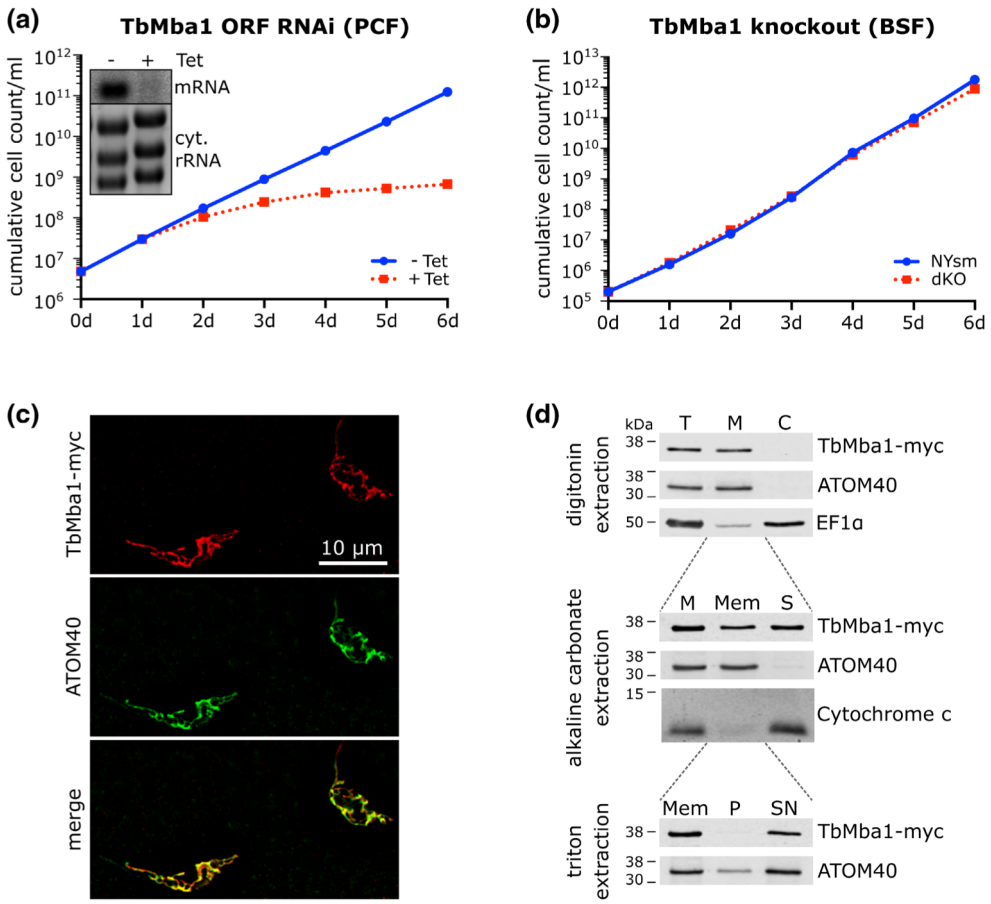

FIGURE 1 (a) Growth curve of uninduced (-Tet) and induced (+Tet) TbMba1 RNAi PCF cell line targeting the ORF of TbMba1. The growth curves were done in triplicates, but the standard deviations are too small to be seen. Inset shows a northern blot of total RNA from uninduced and 2-day induced cells, probed for the ORF of TbMba1. Ethidium bromide stained cytosolic (cyt.) rRNAs serve as loading control. (b) Growth curve of wild-type NYsm BSF cell line and TbMba1 dKO BSF cell line. (c) Immunofluorescence analysis of TbMba1-myc exclusive expressor. ATOM40 serves as a mitochondrial marker. (d) Digitonin extraction: Whole cells (T) of 2-day induced TbMba1-myc exclusive expressor cells were treated with 0.015% digitonin and differential centrifugation to separate a mitochondrial fraction (M) from a cytosolic fraction (C). Immunoblot analysis using anti-myc antibody to detect TbMba1-myc was performed. Anti-ATOM40 and anti-EF1α antibodies were used to detect a mitochondrial and cytosolic control respectively. Alkaline carbonate extraction: A digitonin-extracted mitochondrial fraction was generated and solubilized in an alkaline carbonate extraction at pH 11.5. Differential centrifugation resulted in a pellet (Mem) and soluble (S) fraction that were analysed by immunoblotting. Anti-myc antibody was used to detect TbMba1-myc. Anti-ATOM40 and anti-Cytochrome c antibodies were used as controls for a membrane integral and membrane-associated protein respectively. Triton extraction: Half of the Mem fraction from the alkaline carbonate extraction was solubilized in 1% Triton-X-100. Differential centrifugation resulted in a pellet (P) and soluble (SN) fraction. Immunoblot analysis was performed using anti-myc and anti-ATOM40 antibody.

of TbMba1-myc in the same cell line using immunofluorescence (IF) microscopy. After 2 days of induction, TbMba1-myc localized to the reticulated mitochondrial structure spanning the whole cell of PCF *T. brucei*. The very same structure was also stained by the mitochondrial marker atypical translocase of the outer mitochondrial membrane 40 (ATOM40) (Figure 1c).

Furthermore, the TbMba1-myc exclusive expressor cell line was subjected to a digitonin fractionation, in which a mitochondria-enriched pellet was separated from a soluble fraction enriched in cytosolic proteins. These fractions were analysed by SDS-PAGE and immunoblotting and showed the expected co-fractionation of TbMba1-myc with ATOM40. The cytosolic marker eukaryotic translation elongation factor 1α (EF1α), however, is exclusively detected in the cytosolic fraction, showing successful separation of organelles and cytosol (Figure 1d, top panel). A fraction of the mitochondria-enriched pellet was subjected to an alkaline carbonate extraction at high pH, which allows separation of soluble proteins from membrane-integral proteins. After differential centrifugation, a large fraction of TbMba1-myc was recovered in the soluble fraction together with the peripheral membrane protein marker cytochrome c. However, a significant amount of the protein was also recovered in the membrane fraction (Mem) together with the integral membrane protein ATOM40 (Figure 1d, middle panel). A subsequent Triton-X-100 extraction of the Mem fraction resulted in a complete solubilization of TbMba1-myc, showing that the fraction of TbMba1 present in the Mem sample was not aggregated (Figure 1d, bottom panel). Thus, while most of TbMba1 is soluble, a smaller fraction appears to be associated with the membrane.

In summary, TbMba1 is essential for normal growth in PCF *T. brucei*, but dispensable in the BSF. C-terminally myc-tagged TbMba1 is functional and localizes to the mitochondrion, where it seems to be peripherally associated with the mitochondrial membrane. Thus, it behaves similar as Mba1 of *S. cerevisiae*, which is a peripheral IM protein that faces the matrix (Rep & Grivell, 1996).

2.2.1 | TbMba1 depletion preferentially affects OXPHOS components

In *S. cerevisiae*, Mba1 interacts with the mitoribosome, aligning its exit tunnel with the IM insertase Oxa1, and mediates the integration of OXPHOS subunits into the IM (Ott & Herrmann, 2010). However, the loss of yeast Mba1 only causes a growth defect and inactivation of OXPHOS when Oxa1 is abolished at the same time (Preuss et al., 2001). To determine the effect of TbMba1 ablation on a global level in *T. brucei*, a quantitative proteomic analysis of the steady-state levels of mitochondrial proteins in the TbMba1 ORF RNAi cell line was performed. The cell line was grown under stable isotope labelling by amino acids in cell culture (SILAC) conditions in medium containing different stable isotope-labelled forms of arginine and lysine. After 3 days of induction, equal cell numbers of induced and uninduced cultures, grown in the presence of either light or heavy amino acids, were mixed. Mitochondria-enriched pellets were obtained by digitonin extraction and analysed by quantitative mass spectrometry (MS). All proteins that were detected in at least two of three independent biological replicates and that have previously been identified to be mitochondrial proteins (Peikert et al., 2017; Ramrath et al., 2018; Zíková et al., 2017) are depicted in the volcano plot in Figure 2a. The RNAi target, TbMba1, was downregulated 19-fold in one replicate, but not detected in the other two (Table S1), it is therefore not depicted in the volcano plot. Twenty-three mitochondrial proteins were significantly depleted more than 1.5-fold.

Fourteen of them (61%) are known components of OXPHOS complexes, according to Zíková et al. (2017) (Figure 2a). This corresponds to a relative enrichment of 2.5-fold when compared to all other detected mitochondrial proteins that were significantly depleted more than 1.5-fold. Moreover, 12 of the 14 depleted OXPHOS subunits are subunits of cytochrome c oxidase (Cox), also termed complex IV. Hence, the proteins most affected by downregulation of TbMba1 are predominantly complex IV subunits. Interestingly, none of the MRPs detected in the same analysis was depleted more than 1.5-fold, suggesting that depletion of TbMba1 does not affect the integrity of the mitoribosomes. Of the other eight mitochondrial proteins (35%) that were significantly depleted more than 1.5-fold, one is annotated as a nucleobase/nucleoside transporter 8.2 (Tb927.11.3620), one as a putative pteridine transporter (Tb927.10.9080), one as a putative amino acid transporter (Tb927.8.8300) and five are trypanosomatid-specific proteins of unknown function (Tb927.7.7090, Tb927.10.6200, Tb927.10.4240, Tb927.5.2560, Tb927.11.16510). Depletion of complex IV was verified by analysing solubilized mitochondria-enriched fractions of uninduced and induced TbMba1 ORF RNAi cells by blue native (BN)-PAGE and subsequent immunoblotting using an antiserum specific against CoxIV (Figure 2b). Quantification of triplicate BN-PAGE gels (Figure 2c) revealed a signal that was significantly decreased to 47% after 4 days of RNAi induction. These results support that TbMba1, just as Mba1 in *S. cerevisiae*, is involved in the biogenesis of OXPHOS complexes.

To exclude that the observed loss of OXPHOS subunits is due to a possibly indirect decrease of mitochondrial protein import, whole cell samples were harvested every day over a 6-day period after TbMba1 ORF RNAi induction and analysed by SDS-PAGE and immunoblotting. CoxIV contains an N-terminal presequence that is cleaved off after successful import, resulting in a shorter mature protein. Accumulation of uncleaved CoxIV precursor in the cytosol is an established hallmark of a mitochondrial protein import defect (Harsman et al., 2016; von Känel et al., 2020; Wenger et al., 2017). CoxIV immunoblots of whole cell extracts revealed an accumulation of CoxIV precursor after 5 days of TbMba1 ORF RNAi induction (Figure 2d), 3 days after the onset of the growth phenotype (Figure 1a). This means that the subunits of the OXPHOS complexes, including the ones of complex IV, are depleted well before a mitochondrial protein import defect is seen (Figure 2a–c). Thus, TbMba1 seems to have a direct role in the biogenesis of OXPHOS subunits, but is not involved in mitochondrial protein import.

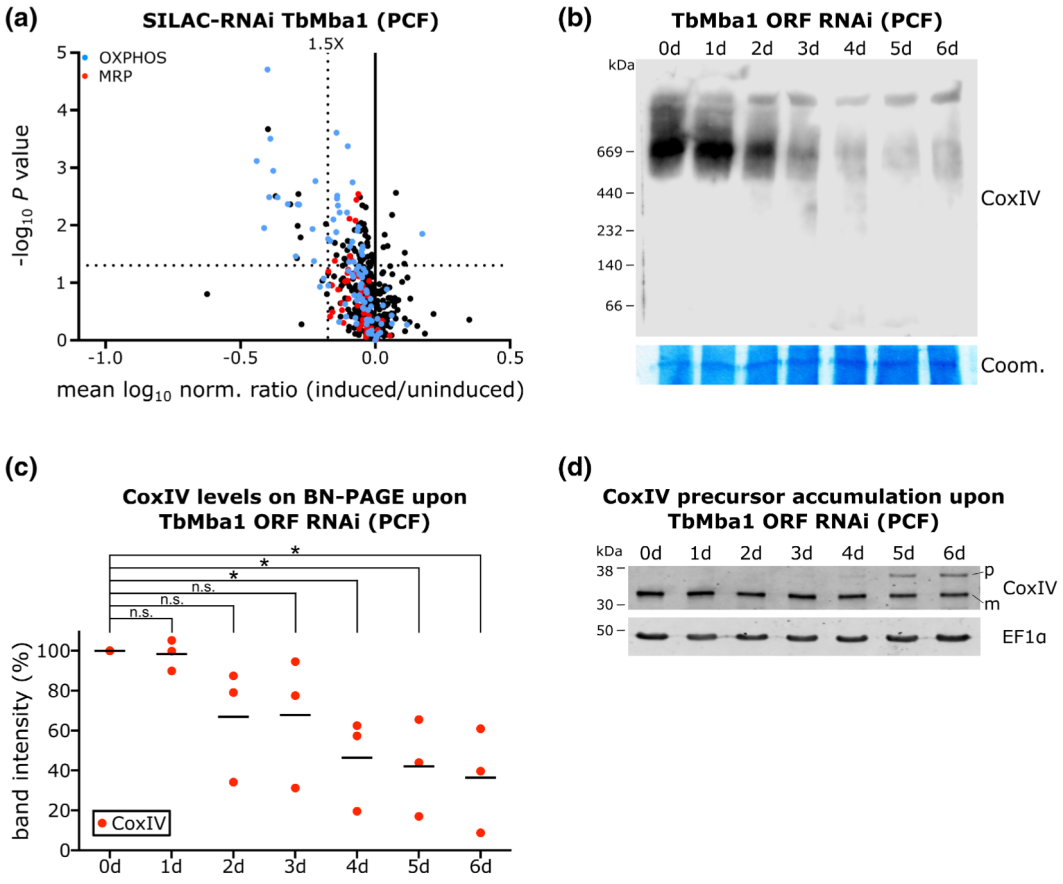

FIGURE 2 (a) Mitochondria-enriched extracts of uninduced and 3-day induced TbMba1 ORF RNAi PCF cells, grown under SILAC-conditions, were mixed and analysed by quantitative MS. The volcano plot shows the mean $\log_{10}$ of the normalized (norm.) ratio (induced/uninduced) of mitochondrial proteins that were detected in at least two of three independent biological replicates, plotted against the corresponding $-\log_{10}$ *P* values (two-sided t-test). TbMba1 was only detected in one replicate and does not appear in the volcano plot. The vertical dotted line indicates 1.5-fold depletion. The horizontal dotted line indicates a t-test significance level of 0.05. In this experiment only, a single non-mitochondrial protein (Histone H3) was significantly depleted more than 1.5-fold (Table S1). (b) BN-PAGE and immunoblot analysis of complex IV in the TbMba1 ORF RNAi PCF cell line. Mitochondria-enriched fractions were prepared after 0–6 days of RNAi induction and separated on a BN-PAGE. Complex IV was detected by probing with anti-CoxIV antibody. Coomassie (Coom.) serves as loading control. (c) Densitometric quantification of CoxIV signals as shown on BN-PAGE in B. Three independent biological replicates were measured. The levels of uninduced cells (0d) were set to 100%, the mean for each day is indicated. Significance was determined by a one-way ANOVA (*p* value = .0199) and post hoc two-tailed independent samples t-tests (n.s.: not significant, **p* value < .05) (d) Whole cell extracts were harvested over 0–6 days of TbMba1 ORF RNAi induction and analysed by SDS-PAGE and immunoblotting, using anti-CoxIV and anti-EF1α antibodies. The precursor (p) and mature (m) forms of CoxIV are indicated and EF1α serves as a loading control.

The biogenesis of OXPHOS complexes relies on the proper translation of mitochondrially encoded subunits of OXPHOS complexes by the mitoribosome. Thus, similar phenotypes as the ones observed after downregulation of TbMba1 might also be expected when we directly interfere with mitochondrial translation. To test this, we knocked down TbMRPL22, a protein of the large subunit of the mitoribosome. Figure 3a shows that as expected for an MRP, this causes a growth retardation starting 3 days after induction. A SILAC-RNAi experiment with the TbMRPL22 ORF RNAi cell line, using the same procedure as explained above for the TbMba1 SILAC RNAi was done. The cells were harvested on day 3 after induction. All proteins that were detected in at least two of three independent biological replicates and that have previously been identified to be mitochondrial proteins (Peikert et al., 2017; Ramrath et al., 2018; Zíková et al., 2017) are depicted in the volcano plot in Figure 3b. TbMRPL22, the target of the RNAi, is efficiently downregulated more than 10-fold (Table S2). Moreover, 52 mitochondrial proteins were significantly depleted more than 1.5-fold. 29 (56%) of these proteins are MRPs, 28 of the mt-LSU and one of the small subunit of the mitoribosome. This suggests that, in contrast to TbMba1 ablation, depletion of TbMRPL22 affects the integrity of the mitoribosomes. Of the remaining 23 proteins, 11 are OXPHOS subunits, of which nine belong to complex IV. Thus, the relative enrichments of OXPHOS subunits and MRPs of the mt-LSU that were significantly depleted more than 1.5-fold by TbMRPL22 RNAi were 1.5 and 3.6-fold, respectively, when compared to all other mitochondrial proteins. Thus, in regard to OXPHOS components, ablation of TbMRPL22 essentially matches the effects seen after depletion of TbMba1.

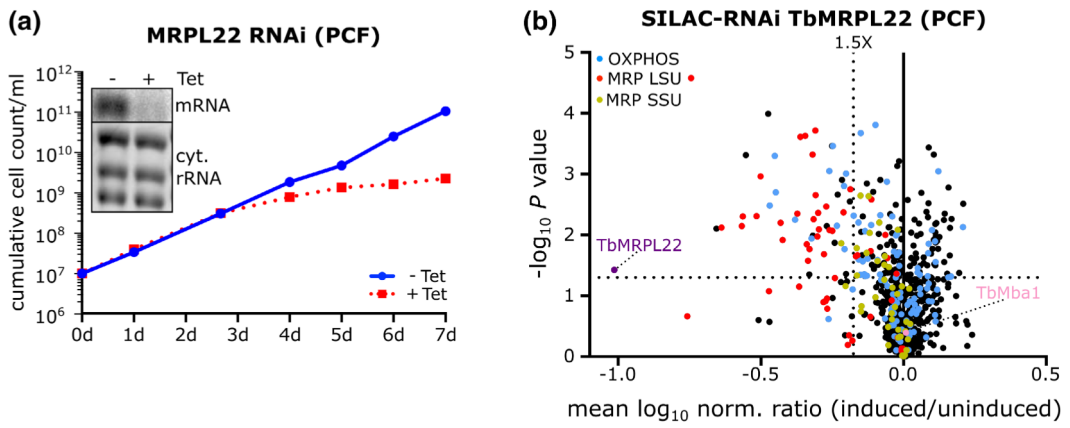

FIGURE 3 (a) Growth curve of uninduced (-Tet) and induced (+Tet) TbMRPL22 RNAi PCF cell line targeting the ORF of TbMRPL22. The growth curves were done in triplicates, but the standard deviations are too small to be seen. Inset shows northern blot of total RNA from uninduced and 2 days induced cells, probed for the ORF of TbMRPL22. Ethidium bromide stained cytosolic (cyt.) rRNAs serve as loading control. (b) Mitochondria-enriched extracts of uninduced and 3-day induced TbMRPL22 ORF RNAi PCF cells, grown under SILAC-conditions, were mixed and analysed by quantitative MS. The volcano plot shows the mean $\log_{10}$ of the normalized (norm.) ratio (induced/uninduced) of mitochondrial proteins that were detected in at least two of three independent biological replicates, plotted against the corresponding $-\log_{10}$ *P* values (two-sided t-test). Proteins involved in OXPHOS and proteins of the large (MRP LSU) and small subunit of the mitoribosome (MRP SSU) are indicated by colours. The position of TbMba1 is indicated in pink. The vertical dotted line indicates 1.5-fold depletion. The horizontal dotted line indicates a t-test significance level of 0.05. In this experiment, two putative non-mitochondrial proteins (Tb927.4.830, Tb927.8.6000) were significantly depleted more than 1.5-fold (Table S2).

As discussed above, depletion of TbMba1 only marginally affects the levels of MRPs suggesting that the mitoribosomes are still intact. This allows to investigate whether they are still associated with the mitochondrial IM. To that end, we produced two TbMba1 ORF RNAi cell lines expressing in situ HA-tagged MRPs mL78 (mL78-HA) or L20 (L20-HA) respectively (Figure 4a,b). Mitochondria-enriched pellets of these two cell lines, obtained by digitonin extraction, were subjected to 15 freeze–thaw cycles followed by differential centrifugation to obtain a membrane (Mem) and a matrix (Mat) fraction. Subsequently, the fractions were analysed by SDS-PAGE and immunoblotting. The matrix protein TbmHsp70 and the IM protein TbTim17 were used as the matrix and membrane markers respectively. Interestingly, both mL78-HA and L20-HA remained predominantly in the membrane fraction in both uninduced and up to 6 days induced cells. Thus, depletion of Mba1 is not sufficient to abolish the membrane association of trypanosomal mitoribosomes (Figure 4c). This suggests that *T. brucei* mitoribosomes use multiple factors to associate with the IM (Pyrih et al., 2021) as is the case in *S. cerevisiae* (Bauerschmitt et al., 2010; Keil et al., 2012). The essential function of TbMba1 goes therefore beyond contributing to a physical connection that associates the mitoribosome to the IM.

In summary, ablation of TbMba1 in PCF *T. brucei* causes the depletion of OXPHOS components with a preference for complex IV subunits. This phenotype can be mimicked when mitochondrial translation is directly abolished by knockdown of the MRP TbMRPL22. Knockdown of TbMba1, however, does neither affect steady-state levels of MRPs nor the physical connection of the mitoribosome with the IM.

2.2.2 | TbMba1 interacts transiently with TbLetm1 and Tb927.11.16250

To find possible interaction partners, a SILAC-based quantitative MS analysis of a co-immunoprecipitation (SILAC-CoIP) was performed using the cell line that exclusively expresses TbMba1-myc (Figure S2c). In order to identify proteins that stably interact with TbMba1, equal cell numbers of uninduced and 2 days induced cultures, grown in the presence of either light or heavy isotope-containing arginine and lysine, were mixed. Subsequently, mitochondria-enriched fractions were generated, solubilized and subjected to CoIP. The eluates were analysed by quantitative MS and all mitochondrial proteins (Peikert et al., 2017; Ramrath et al., 2018; Zíková et al., 2017) that were detected in at least two of three independent biological replicates are depicted in the volcano plot in Figure 5a. The bait TbMba1 was enriched 98-fold demonstrating that the CoIP has worked (Table S3). However, no other protein was enriched more than fivefold indicating that TbMba1 does not efficiently form a stable complex with other proteins. This result is supported by the fact that no high molecular weight complex was detected when a solubilized, mitochondria-enriched fraction of the TbMba1-myc exclusive expressor cell line was analysed by BN-PAGE (Figure S3).

The SILAC-CoIP approach explained above includes the mixing of differently labelled uninduced and induced cells prior to the CoIP. In this so-called premix approach, transient but specific interaction partners of TbMba1-myc may elude detection due to molecular rearrangements between heavy or light labelled proteins bound to the bait during purification (Oeljeklaus et al., 2012). To

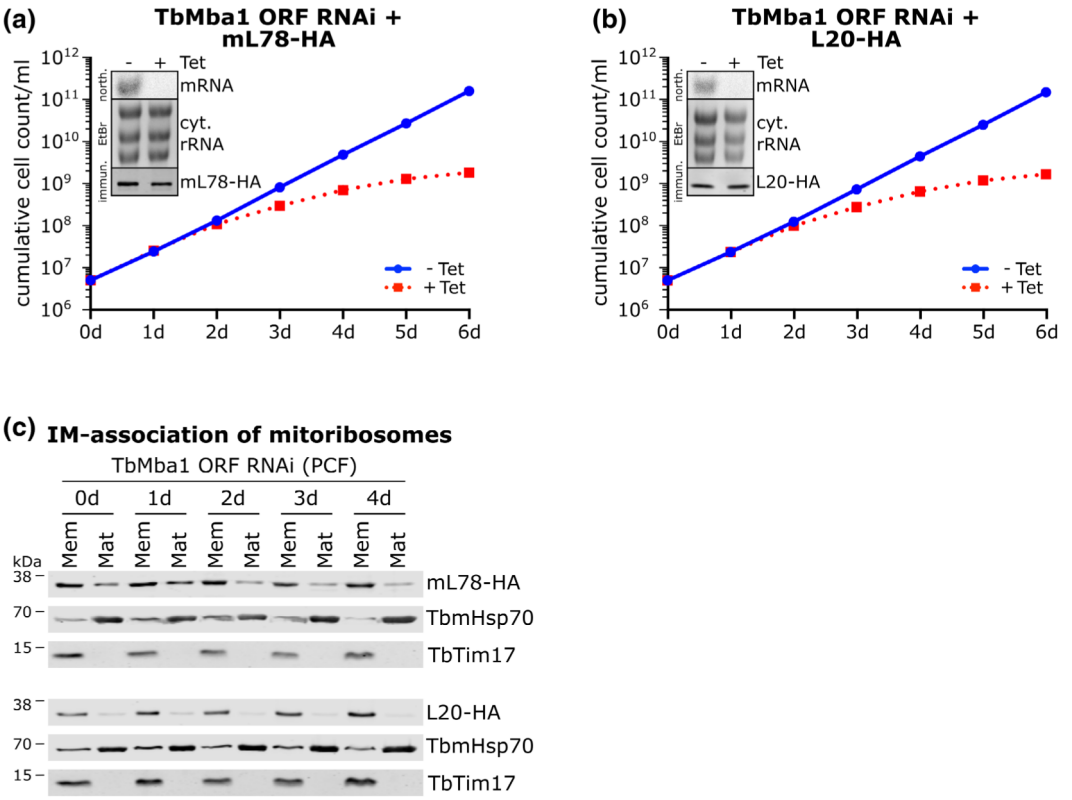

FIGURE 4 (a) Growth curve of uninduced (-Tet) and induced (+Tet) TbMba1 RNAi PCF cell line targeting the ORF of TbMba1 in the background of mL78-HA in situ expression. The growth curves were done in triplicates, but the standard deviations are too small to be seen. Inset shows northern blot (north.) of total RNA from uninduced and 2-day induced cells, probed for the ORF of TbMba1. Ethidium bromide (EtBr) stained cytosolic (cyt.) rRNAs serve as loading control. Immunoblot (immun.) analysis of whole cell extracts, probed with anti-HA antibody, to show expression of mL78-HA. (b) As in (a), but L20-HA is in situ expressed instead of mL78-HA. The growth curves were done in triplicates, but the standard deviations are too small to be seen. (c) Immunoblot analysis of two cell lines, either in situ expressing mL78-HA or L20-HA in the background of TbMba1 ORF RNAi in PCF *T. brucei*. The RNAi was induced from 0 to 4 days and mitochondria-enriched extracts were separated into membrane (Mem) and matrix (Mat) fractions by freeze–thaw cycles. The tagged proteins were detected using anti-HA antibody. Detection with anti-TbmHsp70 and anti-TbTim17 served as matrix and membrane controls respectively.

address this issue, we subjected differentially labelled uninduced and induced cells expressing TbMba1-myc to separate CoIPs and mixed only the resulting eluates. This so-called postmix approach allows for the detection of transient interactions. The result is shown in the volcano plot in Figure 5b, which depicts all mitochondrial proteins (Peikert et al., 2017) that were detected in at least two of three independent biological replicates. Again, the bait TbMba1 was 100-fold enriched (Table S3). Moreover, six proteins were enriched between 5- and 10-fold. One of the enriched proteins was previously identified as TbLetm1 (Tb927.3.4920), the *T. brucei* orthologue of yeast Mdm38 (Hashimi et al., 2013). This is in line with the observation that in yeast, Mba1 and Mdm38 are interaction partners (Bauerschmitt et al., 2010) and suggests TbLetm1/Mdm38 might be involved in the biogenesis of mitochondrially encoded OXPHOS components. This is a novel function for TbLetm1 which was previously shown to be involved in K^+/H^+ homoeostasis (Hashimi et al., 2013; Nowikovsky et al., 2007). Intriguingly the latter function is also carried out by yeast Mdm38 (Lupo et al., 2011; Zhang et al., 2019). Thus, it is likely that TbLetm1 and yeast Mdm38 are functionally conserved.

Another previously characterized protein that was enriched about 10-fold was the trypanosome-specific Tb927.11.16250 (Pusnik & Schneider, 2012) which contains two pentatricopeptide repeats (PPR) (150–210 aa) (Mingler et al., 2006). PPR proteins are sequence-specific RNA-binding proteins that are involved in organellar gene expression in all eukaryotes (Schmitz-Linneweber & Small, 2008). In line with this, Tb927.11.16250 selectively stabilizes the mRNAs of mitochondrially encoded CoxI and CoxII (Pusnik & Schneider, 2012). Recent BLAST searches show that Tb927.11.16250 also contains a PilT N-terminus (PIN) domain (355–550 aa), which in many cases has endoribonuclease activity. Other enriched proteins include the trypanosomatid-specific mitochondrial proteins of unknown function Tb927.1.790, Tb927.10.9280 and Tb927.3.2010 (Figure 5b). The SILAC pull-down experiments also recovered a few cytosolic proteins (Figure S4). Since Mba1 is a mitochondria-specific protein, these putative non-mitochondrial interactors were considered as physiologically non-relevant.

In summary, even though TbMba1 does not form a stable complex with other proteins, it transiently interacts with other proteins

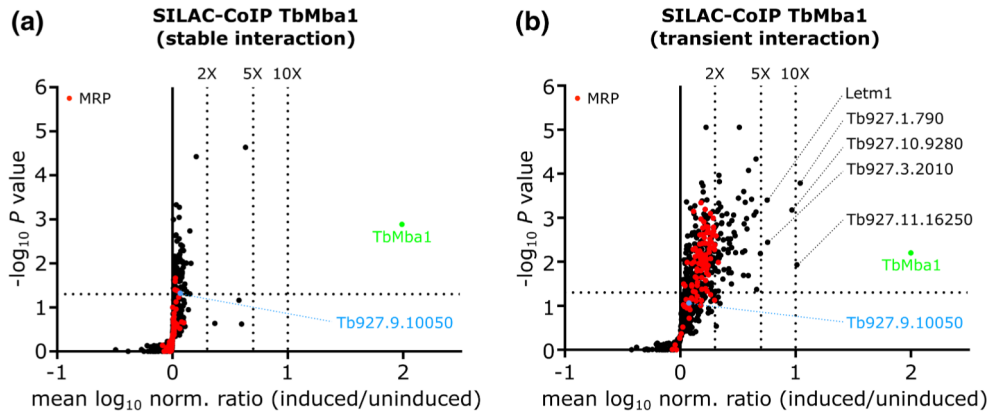

FIGURE 5 (a) Volcano plot of data obtained by SILAC-based quantitative MS analysis of TbMba1-myc CoIPs, performed with mitochondria-enriched extracts. The induced and uninduced cells were mixed prior to performing the CoIP to detect stable interactions. The volcano plot shows the mean $\log_{10}$ of the normalized (norm.) ratio (induced/uninduced) of mitochondrial proteins that were detected in at least two of three independent biological replicates, plotted against the corresponding $-\log_{10}$ *P* values (one-sided t-test). TbMba1, the bait of the SILAC CoIP, was enriched 98-fold. The vertical dotted lines specify the indicated enrichment factors. The horizontal dotted line indicates a t-test significance level of 0.05. MRPs are highlighted in red and the position of the in the only trypanosomal Oxa1 homologue (Tb927.9.10050) detected in this experiment is indicated in blue. (b) Volcano plot of SILAC-based quantitative MS analysis of TbMba1-myc CoIP as in (a), except the CoIPs with induced and uninduced cells were performed separately and the eluates were only mixed prior to MS analysis to detect transient interactions. TbMba1 was enriched 100-fold. The vertical dotted lines specify the indicated enrichment factors. The horizontal dotted line indicates a t-test significance level of 0.05. MRPs are highlighted in red and the position of the only trypanosomal Oxa1 homologue (Tb927.9.10050) detected in this experiment is indicated in blue.

which likely include TbLetm1 and CoxI/CoxII mRNA stabilization factor Tb927.11.16250.

3 | DISCUSSION

The IM is a particularly protein-rich membrane and contains the five protein complexes of the OXPHOS pathway responsible for ATP production, the most iconic function of mitochondria. The majority of the subunits of the OXPHOS complexes is encoded in the nucleus, synthesized in the cytosol and imported into mitochondria, like most other mitochondrial proteins. However, genes encoding the enzymatic core subunits of the OXPHOS system are often retained in the mtDNA (Roger et al., 2017) and the corresponding proteins are co-translationally inserted into the IM by membrane-associated mitoribosomes (Ott & Herrmann, 2010). In *S. cerevisiae*, the interaction of the mitoribosomes with the IM is mediated by at least four factors: the insertase Oxa1 (Jia et al., 2003) via its C-terminus, the IM-associated Mba1 (Ott et al., 2006) and the two integral IM proteins Mdm38 (Frazier et al., 2006) and Mrx15 (Möller-Hergt et al., 2018). Moreover, the expansion segment 96-ES1 of the mitochondrial 21 S rRNA has also been shown to form a contact site with the IM (Pfeffer et al., 2015). The four proteins mentioned above are widely conserved in a broad spectrum of eukaryotes, indicating that they might already have been present in the last eukaryotic common ancestor (LECA) (Pyrih et al., 2021).

Here, we present a functional analysis of the trypanosomal Mba1 orthologue TbMba1. We show that TbMba1, as its yeast counterpart (Rep & Grivell, 1996), is a mitochondrially localized peripheral membrane protein. However, in contrast to yeast Mba1, whose absence resulted in a reduced growth rate on non-fermentable carbon sources only (Rep & Grivell, 1996), depletion of TbMba1 caused a strong reduction of growth of PCF *T. brucei* grown under standard condition in medium containing glucose (Schönenberger & Brun, 1979). This suggests that in PCF *T. brucei*, TbMba1 has a more important role than yeast Mba1, possibly compensating for the absence of a Mrx15 orthologue which surprisingly has not been detected in Euglenozoa (Pyrih et al., 2021), a subgroup of the Discoba which includes *T. brucei* (Burki et al., 2020), even though it is found in essentially all other eukaryotic groups.

Depletion of TbMba1 causes reduced levels of many components of the OXPHOS system most of which are subunits of complex IV. The high sensitivity of complex IV to reduced TbMba1 levels can be explained by the fact that the *T. brucei* mitochondrial genome encodes three of its subunits (Cox I, II and III), whereas for the cytochrome bc1 complex, also termed complex III, and ATP synthase, also termed complex V, only a single subunit each is mitochondrially encoded. Interestingly, the steady-state levels of MRPs remain unchanged in the absence of TbMba1 and so does the IM-association of the mitoribosomes. This suggests that the essential role of TbMba1 in PCF *T. brucei* is not connected to the integrity of the mitoribosomes but directly related to the co-translational integration of newly synthesized mitochondrially encoded proteins into the IM. This also indicates that while TbMba1 might contribute to the maintenance of a physical connection between mitoribosomes and the IM, this function is not essential.

Deleting both alleles of the TbMba1 gene does not affect the growth of BSF trypanosomes. This makes sense since BSF *T. brucei* does not express respiratory complexes I–IV and therefore cannot perform OXPHOS. Instead, BSF cells produce their ATP via glycolysis

(Matthews, 2005; Vickerman, 1985). Thus, no co-translational integration into the IM of mitochondrially encoded subunits of OXPHOS complexes is necessary. However, complex V is an exception, it is essential also in the BSF, not as an ATP synthase but as an enzyme that consumes ATP to maintain the membrane potential (Nolan & Voorheis, 1992; Schnaufer et al., 2005). ATP synthase subunit a, also termed subunit 6, an essential component of the F_o moiety of the ATP synthase, is mitochondrially encoded and therefore must be inserted into the IM even in the absence of TbMba1. In yeast, IM insertion of ATPase subunit 6 is mainly mediated by Mdm38 in concert with Oxa1. Since orthologues of these two proteins are found in the *T. brucei* mitochondrion, the same may be the case for the trypanosomal ATP synthase subunit a.

The mitoribosomes of trypanosomes are very unusual. They have among the shortest known rRNAs of any translation system and 127 MRPs, a number that is much higher than that of any other ribosome (Jaskolowski et al., 2020; Ramrath et al., 2018; Saurer et al., 2019; Soufari et al., 2020; Tobiasson et al., 2021). Half of these proteins are specific for trypanosomes and its relatives. However, uL22 and uL29, the two MRPs that have been previously shown to cross-link to yeast Mba1 (Bieri et al., 2018; de Silva et al., 2015; Gruschke et al., 2010), are conserved in *T. brucei* and contribute to the shape of the exit tunnel region of the trypanosomal mitoribosome (Ramrath et al., 2018). The same is the case for uL23 and uL24, which in yeast were shown to directly interact with the Oxa1 insertase (Bieri et al., 2018; de Silva et al., 2015; Gruschke et al., 2010; Ramrath et al., 2018). It is possible that the scope for evolutionary change in this region of the highly unique trypanosomal mitoribosome is more restricted to evolutionary change because the association with the IM, which must be maintained for efficient co-translational IM integration, is based on conserved proteins like Mba1 and Oxa1.

Pull-down experiments using the cell line exclusively expressing tagged TbMba1 did not recover any proteins that were more than fivefold enriched suggesting that TbMba1 does not form a stable complex with other proteins. Thus, in agreement with the cryo-EM structure of the trypanosomal mitoribosome, TbMba1 itself is not a component of the mitoribosomes (Ramrath et al., 2018). TbMba1 therefore behaves similar to yeast Mba1 and differs from the mammalian Mba1 orthologue mL45, which is firmly integrated into the large mitoribosomal subunit (Greber et al., 2013). TbMba1, however, transiently interacts with five mitochondrial proteins, all of which were more than fivefold enriched in the postmix pull-down experiment. One of these proteins is TbLetm1, whose yeast orthologue Mdm38 was shown to function in the same processes as Mba1. The other previously characterized factor was Tb927.11.16250, a protein containing two PPR and a PIN domain, whose depletion specifically destabilizes CoxI and CoxII mRNAs (Pusnik & Schneider, 2012). This is in line with the observation that Mdm38 in yeast is involved in the recruitment of mRNA stabilization and translation factors (Bauerschmitt et al., 2010), and suggests that TbLetm1 might be involved in recruitment of Tb927.11.16250. Thus, Mba1, TbLetm1, Tb927.11.16250 (Pusnik & Schneider, 2012) and possibly three other trypanosome-specific proteins of unknown function form a dynamic network that mediates and regulates co-translational insertion of OXPHOS complex subunits.

Thus, despite the unique mitoribosome, the role of trypanosomal Mba1 and possibly Letm1 in mediating co-translational IM insertion of subunits of the OXPHOS system appears to be largely conserved between yeast and trypanosomes. It will be exciting to see how the less conserved RNA stabilization factors and translational regulators in different organisms fit into the dynamic interaction network defined by Mba1.

4 | MATERIALS AND METHODS

4.1 | Transgenic cell lines

Transgenic *T. brucei* cell lines are based on the procyclic form (PCF) strain 29-13 or the bloodstream form (BSF) strain New York single marker (NYsm) (Wirtz et al., 1999). PCF *T. brucei* were grown in SDM-79 at 27°C in the presence of 10% (v/v) foetal calf serum (FCS) (Schönenberger & Brun, 1979). BSF *T. brucei* were grown in HMI-9 at 37°C in the presence of 10% (v/v) FCS and 5% CO_2 (Hirumi & Hirumi, 1989).

RNAi cell lines were prepared using a modified pLew100 vector (Wirtz et al., 1999), in which the phleomycin resistance gene was replaced by a blasticidin resistance gene. This vector allows the insertion of RNAi sequences in opposing directions with a 439 bp spacer fragment in between to form a stem loop. The TbMba1 (Tb927.7.4620) RNAis either target the nucleotides (relative to coding start) 322–756 (ORF) or 844–1094 (3′UTR). The TbMRPL22 (Tb927.7.2760) RNAi targets nucleotides (relative to coding start) 121–621 (ORF). The plasmids were linearized with NotI prior to stable transfection of PCF *T. brucei*. The TbMba1 dKO BSF cell line was generated by amplifying 500 nucleotides long sequences directly adjacent to the 5′ and 3′ ends of the coding sequence. The amplified 5′ and 3′ regions were ligated into pMOTag43M using XhoI/NdeI and BamHI/SacI, respectively, flanking the hygromycin resistance gene. The resulting plasmid was digested using XhoI/SacI prior to stable transfection of NYsm cells to replace the first TbMba1 allele with the hygromycin resistance gene. The second TbMba1 allele was replaced analogically by the blasticidin resistance gene using pBLUESCRIPT II KS+ instead of pMOTag43M.

To generate the TbMba1-myc exclusive expressor, first, a triple c-myc tagged variant of TbMba1 was produced (TbMba1-myc). The ORF of TbMba1, excluding the stop codon, was amplified by PCR and ligated into a modified pLew100 vector, containing a C-terminal triple c-myc tag and a stop codon. This plasmid was linearized with NotI prior to stable transfection into the 3′ UTR RNAi cell line of TbMba1. Since the ectopically expressed TbMba1-myc does not contain the endogenous 3′ UTR, it is resistant to the 3′ UTR RNAi. The exclusive expressor cell line was induced with tetracycline 2 days before

experiments to give the RNAi enough time to take effect. The in situ HA-tagged mL78 (Tb927.10.11050) and L20 (Tb927.11.10170) variants (mL78-HA/L20-HA) were produced according to Oberholzer et al. (2006).

4.2 | RNA extraction and northern blotting

Total RNA was extracted from uninduced and 2 days induced RNAi cells, using acid guanidinium thiocyanate-phenol-chloroform extraction according to Chomczynski and Sacchi (1987). Equal amounts of RNA were separated on a 1% agarose gel containing 20 mM MOPS buffer and 0.5% formaldehyde. Gel-purified PCR products, corresponding to the respective RNAi inserts, were used as templates for the Prime-a-Gene labelling system (Promega) to radioactively label the northern probes.

4.3 | Antibodies

Commercially available primary antibodies used: mouse anti-c-myc (Invitrogen, dilution immunoblot (IB) 1:2000, dilution IF 1:100), mouse anti-HA (Enzo Life Sciences AG, dilution IB 1:5000) and mouse anti-EF1α (Merck Millipore, dilution IB 1:10,000). The polyclonal rabbit anti-ATOM40 (dilution IB 1:10,000, dilution IF 1:1000), polyclonal rabbit anti-Cytochrome c (dilution IB 1:100), polyclonal rabbit anti-CoxIV (dilution WB 1:1000) and polyclonal rat anti-TbTim17 (dilution IB: 1:300) were previously produced in our laboratory (Harsman et al., 2016; Niemann et al., 2013). The monoclonal mouse anti-TbmHsp70 (dilution IB 1:1000) was kindly provided to us by Ken Stuart (Panigrahi et al., 2008). Commercially available secondary antibodies used: goat anti-mouse IRDye 680LT conjugated (LI-COR Biosciences, dilution IB 1:20,000), goat anti-Rabbit IRDye 800CW conjugated (LI-COR Biosciences, dilution IB 1:20,000), goat anti-mouse Alexa Fluor 596 (ThermoFisher Scientific, dilution IF 1:1000), goat anti-rabbit Alexa Fluor 488 (ThermoFisher Scientific, dilution IF 1:1000), HRP-coupled goat anti-mouse (Sigma, dilution IB 1:5000). The BN-PAGE immunoblots were developed using the commercial kits SuperSignal West Pico PLUS or SuperSignal West Femto MAXIMUM.

4.4 | Immunofluorescence microscopy

2×10^6 cells were harvested, washed and resuspended in PBS, and then distributed on slides. They were allowed to settle on the plate for 10 min. After the incubation, they were fixed using 4% paraformaldehyde, and then permeabilized using 0.2% Triton X-100. The slides were incubated with the primary and secondary antibodies, described above, prior to picture acquisition using a DMI6000B microscope equipped with a DFC360 FX monochrome camera and LAS X software (Leica Microsystems).

4.5 | Digitonin extraction

A crude mitochondrial fraction was separated from a crude cytosolic fraction by incubating 1×10^8 cells for 10 min on ice in 20 mM Tris–HCl pH 7.5, 0.6 M sorbitol, 2 mM EDTA containing 0.015% (w/v) digitonin. Centrifugation (5 min, 6800 g, 4°C) separates a mitochondria-enriched pellet from the cytosol-containing supernatant. 2.5×10^6 cell equivalents of each fraction were subjected to SDS-PAGE and immunoblotting to show mitochondrial localization of TbMba1-myc.

4.6 | Alkaline carbonate extraction

To separate soluble from membrane-integral proteins, a mitochondria-enriched pellet, obtained by digitonin extraction, was incubated for 10 min on ice in 100 mM Na_2CO_3 at pH 11.5 and centrifuged (100,000 g, 4°C, 10 min). Equal cell equivalents of each sample were analysed by SDS-PAGE and immunoblotting.

4.7 | Triton extraction

To test whether proteins were aggregated or not, the pellet from an alkaline carbonate extraction was incubated for 10 min on ice in 100 mM Na_2CO_3 at pH 11.5 containing 1% Triton X-100. After centrifugation (100,000 g, 4°C, 10 min), the supernatant and pellet were separated. Equivalents of each sample were analysed by SDS-PAGE and immunoblotting.

4.8 | SILAC RNAi

For the SILAC experiments, the cells were grown for 4 days in SDM-80[30] containing 5.55 mM glucose, 10% dialysed FCS (BioConcept, Switzerland), and either light ($^{12}C_6/^{14}N_\chi$) or heavy ($^{13}C_6/^{15}N_\chi$) isotopes of arginine (1.1 mM) and lysine (0.4 mM) (Euroisotop). Three biological replicates of the light/heavy pair were grown for each experiment. Either the light or heavy culture of each pair was induced with tetracycline 3 days before the harvest of TbMba1 RNAi cells or TbMRPL22 RNAi cells. Two·10^8 cells of the heavy culture were mixed with 2×10^8 cells of the light culture and a mitochondria-enriched pellet was obtained by digitonin extraction as described above. The triplicates were analysed by liquid chromatography-mass spectrometry (LC–MS) as described below.

4.9 | SILAC CoIP

Six light/heavy pairs of the TbMba1-myc exclusive expressor cell line were grown for 4 days in SILAC medium as described above. Two days before harvest, either the light or heavy culture of each pair

was induced with tetracycline. To identify stable interactions, three of the light/heavy pairs were prepared as follows: 2×10^8 cells of the heavy culture were mixed with 2×10^8 cells of the light culture and a mitochondria-enriched pellet was obtained by digitonin extraction as described above. The pellet was solubilized in lysis buffer (20 mM Tris–HCl, pH 7.4, 0.1 mM EDTA, 100 mM NaCl, 10% glycerol, 1% (w/v) digitonin, 1× Protease Inhibitor mix (EDTA-free, Roche)) for 15 min on ice. After centrifugation (20,000 g, 4°C, 15 min), the supernatant was incubated with anti-myc affinity matrix (Roche) for 2 h at 4°C. After incubation, the supernatant was removed, and the resin-bound proteins were eluted by boiling the resin for 5 min in SDS loading buffer (2% SDS (w/v), 62.5 mM Tris–HCl pH 6.8, 7.5% glycerol (v/v), bromophenol blue). The proteins were precipitated using methanol and chloroform and resuspended again in loading buffer. The samples were run 1 cm into a 4–12% NuPAGE BisTris gradient gel (Life Technologies). The proteins were stained using colloidal Coomassie Brilliant Blue and the gel piece containing the proteins was cut out. The proteins in the gel fragments were reduced using 5 mM Bond-Breaker TCEP solution (Thermo Scientific, Product No. 77720), alkylated using 100 mM iodoacetamide (Sigma-Aldrich, Product No. I6125) and digested in-gel with trypsin. The triplicates were then analysed by LC–MS as described below.

To identify transient interactions (Oeljeklaus et al., 2012), the same procedure as above was used, but instead of mixing the cells in the beginning, the eluates of each light/heavy pair were mixed after elution from the anti-myc affinity matrix.

4.10 | LC–MS and data analysis

Mitochondria-enriched fractions obtained from SILAC-labelled tetracycline-induced and -uninduced TbMba1 RNAi or TbMRPL22 RNAi cells were prepared for LC–MS analysis as described before (Eichenberger et al., 2019). In brief, mitochondrial fractions were resuspended in urea buffer (8 M urea/50 mM NH_4HCO_3), followed by reduction and alkylation of cysteine residues, dilution of samples to a final urea concentration of 1.6 M using 50 mM NH_4HCO_3 and tryptic digestion. Peptide mixtures were desalted using StageTips, dried in vacuo and reconstituted in 0.1% (v/v) trifluoroacetic acid. Sample were analysed in technical duplicates by nano-HPLC-ESI-MS/MS on an Orbitrap Elite (Thermo Fisher Scientific) coupled to an UltiMate 3000 RSLCnano HPLC system (Thermo Fisher Scientific), which was equipped with PepMap C18 precolumns (Thermo Scientific; length, 5 mm; inner diameter, 0.3 mm; flow rate, 30 µL/min) and an Acclaim PepMap C18 reversed-phase nano-LC column (Thermo Scientific; length, 500 mm; inner diameter, 75 µm; particle size, 2 µm; pore size, 100 Å; flow rate, 0.25 µL/min). Peptides were separated using a binary solvent system consisting of 4% (v/v) dimethyl sulphoxide (DMSO)/0.1% (v/v) formic acid (FA) (solvent A) and 48% (v/v) methanol/30% (v/v) acetonitrile (ACN)/4% (v/v) DMSO/0.1% (v/v) FA (solvent B). A gradient ranging from 1% to 25% solvent B in 115 min followed by 25–45% B in 110 min, 45–60% B in 50 min, 60–80% B in 20 min, 80–99% B in 10 min and 5 min at 99% B was applied for peptide elution. Peptide mixtures generated in TbMba1-myc SILAC CoIP experiments were analysed by LC–MS using the same instrument setting as described above except that the RSLCnano HPLC was equipped with nanoEase M/Z Symmetry C18 precolumns (Waters; length, 20 mm; inner diameter, 0.18 mm; flow rate, 10 µL/min) and a nanoEase M/Z HSS C18 T3 column (Waters; length, 250 mm; inner diameter, 75 µm; particle size, 1.8 µm; packing density, 100 Å; flow rate, 300 nL/min). Peptides were eluted using 0.1% (v/v) FA (solvent A) and 50% (v/v) methanol/30% (v/v) ACN/0.1% (v/v) FA (solvent B) as solvent system and the following gradient: 7–55% solvent B in 175 min followed by 55–95% B in 35 min and 5 min at 95% B.

Mass spectrometric data were acquired in data-dependent mode, applying the following parameters: mass range of *m/z* 370–1700, resolution of 120,000 (at *m/z* 400), target value of 10^6, maximum injection time of 200 ms for MS survey scans. Up to 25 of the most intense precursor ions ($z \geq +2$) were selected for further fragmentation by low-energy collision-induced dissociation in the linear ion trap with a normalized collision energy of 35%, an activation q of 0.25, an activation time of 10 ms, a target value of 5000, a maximum injection time of 150 ms and a dynamic exclusion time of 45 s.

For protein identification and SILAC-based quantification, MaxQuant/Andromeda (Cox et al., 2011; Cox & Mann, 2008) (versions 1.5.3.12, 1.5.4.0 and 1.6.5.0 for data obtained in TbMba1 RNAi, TbMRPL22 RNAi and TbMba1-myc CoIP experiments respectively) and the fasta file for *T. brucei* TREU927 (downloaded from the TriTryp database; version 8.1) were used. Data were processed using MaxQuant default settings except that protein identification and quantification were based on ≥1 unique peptide and ≥1 ratio count respectively. Lys0/Arg0 were set as light and Lys8/Arg10 as heavy labels. The mean of $\log_{10}$-transformed normalized protein abundance ratios were determined for proteins quantified in ≥2 independent biological replicates per data set and a two-sided (SILAC RNAi experiments) or one-sided (TbMba1-myc CoIP experiments) Student's t-test was performed. Information about the proteins identified and quantified are provided in Tables S1–S3.

4.11 | Blue native-PAGE

To analyse native complexes, a mitochondria-enriched pellet obtained by digitonin extraction was used as starting material. This pellet was solubilized in solubilization buffer (20 mM Tris–HCl pH 7.4, 50 mM NaCl, 10% glycerol, 0.1 mM EDTA) containing 1% (w/v) digitonin and incubated on ice for 15 min. After centrifugation (20,000 g, 4°C, 15 min), the supernatant was separated on 4–13% gels. Before western blotting, the gel was incubated in SDS-PAGE running buffer (25 mM Tris, 1 mM EDTA, 190 mM glycine, 0.05% (w/v) SDS) to facilitate transfer of proteins.

4.12 | IM association of mitoribosomes

To separate a mitochondrial matrix fraction from a mitochondrial membrane fraction, 1.5×10^8 TbMba1 ORF RNAi cells that also

in situ express either mL78-HA or L20-HA were induced for up to 4 days with tetracycline. Mitochondria-enriched pellets were obtained using digitonin extraction as described above. The pellets were resuspended in 150 µL 10 mM $MgCl_2$ and then flash frozen in liquid nitrogen and thawed at 25°C 10 times. After centrifugation (10,000 g, 5 min, 4°C), the supernatant was separated from the pellet, which was resuspended in 150 µL 10 mM $MgCl_2$. 37.5 µL 5× loading buffer (10% SDS (w/v), 312.5 mM Tris–HCl pH 6.8, 12.5% β-mercaptoethanol (v/v), 37.5% glycerol (v/v), bromophenol blue) was added to both fractions and incubated 5 min at 95°C. 15 µL of both fractions were analysed by SDS PAGE and immunoblotting.

AUTHOR CONTRIBUTIONS

Christoph Wenger: Conceptualization; Investigation; Writing - original draft; Methodology. **Anke Harsman**: Conceptualization; Investigation; Writing - review & editing. **Moritz Niemann**: Conceptualization; Investigation; Writing - review & editing. **Silke Oeljeklaus**: Formal analysis; Investigation. **Corinne von Känel**: Writing - original draft; Writing - review & editing; Conceptualization. **Salvatore Calderaro**: Investigation. **Bettina Warscheid**: Writing - review & editing; Supervision; Conceptualization; Funding acquisition. **André Schneider**: Conceptualization; Funding acquisition; Writing - original draft; Writing - review & editing; Supervision.

ACKNOWLEDGEMENTS

We thank Bettina Knapp for technical assistance. Work in the lab of B.W. was supported by Germany's Excellence Strategy (CIBSS – EXC-2189 – Project ID 390939984). Work in the lab of A.S. was supported in part by NCCR RNA & Disease, a National Centre of Competence in Research (grant number 205601) and by project grant SNF 205200 both funded by the Swiss National Science Foundation. Open access funding provided by Universitat Bern.

CONFLICT OF INTEREST

The authors declare no conflict of interest.

DATA AVAILABILITY STATEMENT

All data are contained in the supplementary material section (Tables S1–S3).

ETHICS STATEMENT

This article does not contain any studies with human participants or animals. The authors declare no conflict of interest.

REFERENCES

Bauerschmitt, H., Mick, D.U., Deckers, M., Vollmer, C., Funes, S., Kehrein, K. et al. (2010) Ribosome-binding proteins Mdm38 and Mba1 display overlapping functions for regulation of mitochondrial translation. *Molecular Biology of the Cell*, *21*, 1937–1944.

Betts, H.C., Puttick, M.N., Clark, J.W., Williams, T.A., Donoghue, P.C.J. & Pisani, D. (2018) Integrated genomic and fossil evidence illuminates life's early evolution and eukaryote origin. *Nature Ecology & Evolution*, *2*, 1556–1562.

Bieri, P., Greber, B.J. & Ban, N. (2018) High-resolution structures of mitochondrial ribosomes and their functional implications. *Current Opinion in Structural Biology*, *49*, 44–53.

Burki, F., Roger, A.J., Brown, M.W. & Simpson, A.G.B. (2020) The new tree of eukaryotes. *Trends in Ecology & Evolution*, *35*, 43–55.

Chamata, Y., Watson, K.A. & Jauregi, P. (2020) Whey-derived peptides interactions with ACE by molecular docking as a potential predictive tool of natural ACE inhibitors. *International Journal of Molecular Sciences*, *21*, 864.

Chomczynski, P. & Sacchi, N. (1987) Single-step method of RNA isolation by acid guanidinium thiocyanate-phenol-chloroform extraction. *Analytical Biochemistry*, *162*, 156–159.

Clement, S.L., Mingler, M.K. & Koslowsky, D.J. (2004) An intragenic guide RNA location suggests a complex mechanism for mitochondrial gene expression in *Trypanosoma brucei*. *Eukaryotic Cell*, *3*, 862–869.

Cox, J. & Mann, M. (2008) MaxQuant enables high peptide identification rates, individualized p.p.b.-range mass accuracies and proteome-wide protein quantification. *Nature Biotechnology*, *26*, 1367–1372.

Cox, J., Neuhauser, N., Michalski, A., Scheltema, R.A., Olsen, J.V. & Mann, M. (2011) Andromeda: a peptide search engine integrated into the MaxQuant environment. *Journal of Proteome Research*, *10*, 1794–1805.

Dacks, J.B., Field, M.C., Buick, R., Eme, L., Gribaldo, S., Roger, A.J. et al. (2016) The changing view of eukaryogenesis – fossils, cells, lineages and how they all come together. *Journal of Cell Science*, *129*, 3695–3703.

de Silva, D., Tu, Y.T., Amunts, A., Fontanesi, F. & Barrientos, A. (2015) Mitochondrial ribosome assembly in health and disease. *Cell Cycle*, *14*, 2226–2250.

Desai, N., Brown, A., Amunts, A. & Ramakrishnan, V. (2017) The structure of the yeast mitochondrial ribosome. *Science*, *355*, 528–531.

Eichenberger, C., Oeljeklaus, S., Bruggisser, J., Mani, J., Haenni, B., Kaurov, I. et al. (2019) The highly diverged trypanosomal MICOS complex is organized in a nonessential integral membrane and an essential peripheral module. *Molecular Microbiology*, *112*, 1731–1743.

Figueiredo, L.M., Smith, T.K., Bringaud, F. & Nolan, D.P. (2017) Metabolic reprogramming during the *Trypanosoma brucei* life cycle. *F1000Res*, *6*, F1000Faculty Rev-683.

Frazier, A.E., Taylor, R.D., Mick, D.U., Warscheid, B., Stoepel, N., Meyer, H.E. et al. (2006) Mdm38 interacts with ribosomes and is a component of the mitochondrial protein export machinery. *The Journal of Cell Biology*, *172*, 553–564.

Freel, K.C., Friedrich, A. & Schacherer, J. (2015) Mitochondrial genome evolution in yeasts: an all-encompassing view. *FEMS Yeast Research*, *15*, fov023.

Greber, B.J., Boehringer, D., Leitner, A., Bieri, P., Voigts-Hoffmann, F., Erzberger, J.P. et al. (2013) Architecture of the large subunit of the mammalian mitochondrial ribosome. *Nature*, *505*, 515–519.

Gruschke, S., Gröne, K., Heublein, M., Hölz, S., Israel, L., Imhof, A. et al. (2010) Proteins at the polypeptide tunnel exit of the yeast mitochondrial ribosome. *The Journal of Biological Chemistry*, *285*, 19022–19028.

Harsman, A., Oeljeklaus, S., Wenger, C., Huot, J.L., Warscheid, B. & Schneider, A. (2016) The non-canonical mitochondrial inner membrane presequence translocase of trypanosomatids contains two essential rhomboid-like proteins. *Nature Communications*, *7*, 1–13.

Hashimi, H., McDonald, L., Stříbrná, E. & Lukeš, J. (2013) Trypanosome Letm1 protein is essential for mitochondrial potassium homeostasis. *The Journal of Biological Chemistry*, *288*, 26914–26925.

Hirumi, H. & Hirumi, K. (1989) Continuous cultivation of *Trypanosoma brucei* blood stream forms in a medium containing a low concentration of serum protein without feeder cell layers. *Journal of Parasitology*, *75*, 985–989.

Jaskolowski, M., Ramrath, D.J.F., Bieri, P., Niemann, M., Mattei, S., Calderaro, S. et al. (2020) Structural insights into the mechanism of mitoribosomal large subunit biogenesis. *Molecular Cell*, *79*, 629–644.e4.

Jia, L., Dienhart, M., Schramp, M., McCauley, M., Hell, K. & Stuart, R.A. (2003) Yeast Oxa1 interacts with mitochondrial ribosomes: the importance of the C-terminal region of Oxa1. *The EMBO Journal*, *22*, 6438–6447.

Jumper, J., Evans, R., Pritzel, A., Green, T., Figurnov, M., Ronneberger, O. et al. (2021) Highly accurate protein structure prediction with AlphaFold. *Nature*, *596*, 583–589.

Kaufer, A., Ellis, J., Stark, D. & Barratt, J. (2017) The evolution of trypanosomatid taxonomy. *Parasites & Vectors*, *10*, 1–17.

Keil, M., Bareth, B., Woellhaf, M.W., Peleh, V., Prestele, M., Rehling, P. et al. (2012) Oxa1-ribosome complexes coordinate the assembly of cytochrome C oxidase in mitochondria. *The Journal of Biological Chemistry*, *287*, 34484–34493.

Lamour, N., Rivière, L., Coustou, V., Coombs, G.H., Barrett, M.P. & Bringaud, F. (2005) Proline metabolism in procyclic *Trypanosoma brucei* is down-regulated in the presence of glucose. *The Journal of Biological Chemistry*, *280*, 11902–11910.

Lupo, D., Vollmer, C., Deckers, M., Mick, D.U., Tews, I., Sinning, I. et al. (2011) Mdm38 is a 14-3-3-like receptor and associates with the protein synthesis machinery at the inner mitochondrial membrane. *Traffic*, *12*, 1457–1466.

Madeira, F., Pearce, M., Tivey, A.R.N., Basutkar, P., Lee, J., Edbali, O. et al. (2022) Search and sequence analysis tools services from EMBL-EBI in 2022. *Nucleic Acids Research*, *1*, W276–W279.

Mani, J., Desy, S., Niemann, M., Chanfon, A., Oeljeklaus, S., Pusnik, M. et al. (2015) Mitochondrial protein import receptors in Kinetoplastids reveal convergent evolution over large phylogenetic distances. *Nature Communications*, *6*, 1–12.

Mantilla, B.S., Marchese, L., Casas-Sánchez, A., Dyer, N.A., Ejeh, N., Biran, M. et al. (2017) Proline metabolism is essential for *Trypanosoma brucei* survival in the tsetse vector. *PLoS Pathogens*, *13*, e1006158.

Matthews, K.R. (2005) The developmental cell biology of *Trypanosoma brucei*. *Journal of Cell Science*, *118*, 283–290.

McDowell, M.A., Heimes, M. & Sinning, I. (2021) Structural and molecular mechanisms for membrane protein biogenesis by the Oxa1 superfamily. *Nature Structural & Molecular Biology*, *28*, 234–239.

Mingler, M.K., Hingst, A.M., Clement, S.L., Yu, L.E., Reifur, L. & Koslowsky, D.J. (2006) Identification of pentatricopeptide repeat proteins in *Trypanosoma brucei*. *Molecular and Biochemical Parasitology*, *150*, 37–45.

Möller-Hergt, B.V., Carlström, A., Stephan, K., Imhof, A. & Ott, M. (2018) The ribosome receptors Mrx15 and Mba1 jointly organize cotranslational insertion and protein biogenesis in mitochondria. *Molecular Biology of the Cell*, *29*, 2386–2396.

Niemann, M., Wiese, S., Mani, J., Chanfon, A., Jackson, C., Meisinger, C. et al. (2013) Mitochondrial outer membrane proteome of *Trypanosoma brucei* reveals novel factors required to maintain mitochondrial morphology. *Molecular & Cellular Proteomics*, *12*, 515–528.

Nolan, D.P. & Voorheis, H.P. (1992) The mitochondrion in bloodstream forms of *Trypanosoma brucei* is energized by the electrogenic pumping of protons catalysed by the F1F0-ATPase. *European Journal of Biochemistry*, *209*, 207–216.

Nowikovsky, K., Reipert, S., Devenish, R.J. & Schweyen, R.J. (2007) Mdm38 protein depletion causes loss of mitochondrial K+/H+ exchange activity, osmotic swelling and mitophagy. *Cell Death and Differentiation*, *14*, 1647–1656.

Oberholzer, M., Morand, S., Kunz, S. & Seebeck, T. (2006) A vector series for rapid PCR-mediated C-terminal in situ tagging of *Trypanosoma brucei* genes. *Molecular and Biochemical Parasitology*, *145*, 117–120.

Oeljeklaus, S., Reinartz, B.S., Wolf, J., Wiese, S., Tonillo, J., Podwojski, K. et al. (2012) Identification of core components and transient interactors of the peroxisomal importomer by dual-track stable isotope labeling with amino acids in cell culture analysis. *Journal of Proteome Research*, *11*, 2567–2580.

Ott, M. & Herrmann, J.M. (2010) Co-translational membrane insertion of mitochondrially encoded proteins. *Biochimica et Biophysica Acta*, *1803*, 767–775.

Ott, M., Prestele, M., Bauerschmitt, H., Funes, S., Bonnefoy, N. & Herrmann, J.M. (2006) Mba1, a membrane-associated ribosome receptor in mitochondria. *The EMBO Journal*, *25*, 1603–1610.

Panigrahi, A.K., Zíková, A., Dalley, R.A., Acestor, N., Ogata, Y., Anupama, A. et al. (2008) Mitochondrial complexes in *Trypanosoma brucei*: a novel complex and a unique oxidoreductase complex. *Molecular & Cellular Proteomics*, *7*, 534–545.

Peikert, C.D., Mani, J., Morgenstern, M., Käser, S., Knapp, B., Wenger, C. et al. (2017) Charting organellar importomes by quantitative mass spectrometry. *Nature Communications*, *8*, 15272.

Pfeffer, S., Woellhaf, M.W., Herrmann, J.M. & Förster, F. (2015) Organization of the mitochondrial translation machinery studied in situ by cryoelectron tomography. *Nature Communications*, *6*, 6019.

Preuss, M., Leonhard, K., Hell, K., Stuart, R.A., Neupert, W. & Herrmann, J.M. (2001) Mba1, a novel component of the mitochondrial protein export machinery of the yeast Saccharomyces cerevisiae. *The Journal of Cell Biology*, *153*, 1085–1095.

Pusnik, M. & Schneider, A. (2012) A trypanosomal pentatricopeptide repeat protein stabilizes the mitochondrial mRNAs of cytochrome oxidase subunits 1 and 2. *Eukaryotic Cell*, *11*, 79–87.

Pyrih, J., Pánek, T., Durante, I.M., Rašková, V., Cimrhanzlová, K., Kriegová, E. et al. (2021) Vestiges of the bacterial signal recognition particle-based protein targeting in mitochondria. *Molecular Biology and Evolution*, *38*, 3170–3187.

Ramrath, D.J.F., Niemann, M., Leibundgut, M., Bieri, P., Prange, C., Horn, E.K. et al. (2018) Evolutionary shift toward protein-based architecture in trypanosomal mitochondrial ribosomes. *Science (1979)*, *362*, eaau7735.

Rep, M. & Grivell, L.A. (1996) MBA1 encodes a mitochondrial membrane-associated protein required for biogenesis of the respiratory chain. *FEBS Letters*, *388*, 185–188.

Rep, M., Nooy, J., Guélin, E. & Grivell, L.A. (1996) Three genes for mitochondrial proteins suppress null-mutations in both Afg3 and Rca1 when over-expressed. *Current Genetics*, *30*, 206–211.

Roger, A.J., Muñoz-Gómez, S.A. & Kamikawa, R. (2017) The origin and diversification of mitochondria. *Current Biology*, *27*, 1177–1192.

Saurer, M., Ramrath, D.J.F., Niemann, M., Calderaro, S., Prange, C., Mattei, S. et al. (2019) Mitoribosomal small subunit biogenesis in trypanosomes involves an extensive assembly machinery. *Science*, *365*, 1144–1149.

Schmitz-Linneweber, C. & Small, I. (2008) Pentatricopeptide repeat proteins: a socket set for organelle gene expression. *Trends in Plant Science*, *13*, 663–670.

Schnaufer, A., Clark-Walker, G.D., Steinberg, A.G. & Stuart, K. (2005) The F1-ATP synthase complex in bloodstream stage trypanosomes has an unusual and essential function. *The EMBO Journal*, *24*, 4029–4040.

Schneider, A. (2020) Evolution of mitochondrial protein import – lessons from trypanosomes. *Biological Chemistry*, *401*, 663–676.

Schneider, A. (2022) Evolution and diversification of mitochondrial protein import systems. *Current Opinion in Cell Biology*, *75*, 102077.

Schönenberger, M. & Brun, R. (1979) Cultivation and in vitro cloning of procyclic culture forms of '*Trypanosoma brucei*' in a semi-defined medium: short communication. *ActaTropica*, *36*, 289–292.

Scotti, P.A., Urbanus, M.L., Brunner, J., de Gier, J.W.L., von Heijne, G., van der Does, C. et al. (2000) YidC, the Escherichia coli homologue of mitochondrial Oxa1p, is a component of the sec translocase. *The EMBO Journal*, *19*, 542–549.

Soufari, H., Waltz, F., Parrot, C., Durrieu-Gaillard, S., Bochler, A., Kuhn, L. et al. (2020) Structure of the mature kinetoplastids mitoribosome and insights into its large subunit biogenesis. *Proceedings of the National Academy of Sciences of the United States of America*, *117*, 29851–29861.

Spang, A., Saw, J.H., Jørgensen, S.L., Zaremba-Niedzwiedzka, K., Martijn, J., Lind, A.E. et al. (2015) Complex archaea that bridge the gap between prokaryotes and eukaryotes. *Nature*, *521*, 173–179.

Tobiasson, V., Gahura, O., Aibara, S., Baradaran, R., Zíková, A. & Amunts, A. (2021) Interconnected assembly factors regulate the biogenesis of mitoribosomal large subunit. *The EMBO Journal*, *40*, e106292.

Urbaniak, M.D., Guther, M.L.S. & Ferguson, M.A.J. (2012) Comparative SILAC proteomic analysis of *Trypanosoma brucei* bloodstream and procyclic lifecycle stages. *PLoS One*, *7*, e36619.

Varadi, M., Anyango, S., Deshpande, M., Nair, S., Natassia, C., Yordanova, G. et al. (2022) AlphaFold protein structure database: massively expanding the structural coverage of protein-sequence space with high-accuracy models. *Nucleic Acids Research*, *50*, D439–D444.

Verner, Z., Basu, S., Benz, C., Dixit, S., Dobáková, E., Faktorová, D. et al. (2015) Malleable mitochondrion of *Trypanosoma brucei*. *International Review of Cell and Molecular Biology*, *315*, 73–151.

Vickerman, K. (1985) Developmental cycles and biology of pathogenic trypanosomes. *British Medical Bulletin*, *41*, 105–114.

von Känel, C., Muñoz-Gómez, S.A., Oeljeklaus, S., Wenger, C., Warscheid, B., Wideman, J.G. et al. (2020) Homologue replacement in the import motor of the mitochondrial inner membrane of trypanosomes. *eLife*, *9*, e52560.

Wang, Z. & Wu, M. (2015) An integrated phylogenomic approach toward pinpointing the origin of mitochondria. *Scientific Reports*, *5*, 7949.

Wenger, C., Oeljeklaus, S., Warscheid, B., Schneider, A. & Harsman, A. (2017) A trypanosomal orthologue of an intermembrane space chaperone has a non-canonical function in biogenesis of the single mitochondrial inner membrane protein translocase. *PLoS Pathogens*, *13*, e1006550.

Wirtz, E., Leal, S., Ochatt, C. & Cross, G.A.M. (1999) A tightly regulated inducible expression system for conditional gene knock-outs and dominant-negative genetics in *Trypanosoma brucei*. *Molecular and Biochemical Parasitology*, *99*, 89–101.

Wolters, J.F., Chiu, K. & Fiumera, H.L. (2015) Population structure of mitochondrial genomes in Saccharomyces cerevisiae. *BMC Genomics*, *16*, 451.

Zaremba-Niedzwiedzka, K., Caceres, E.F., Saw, J.H., Bäckström, D., Juzokaite, L., Vancaester, E. et al. (2017) Asgard archaea illuminate the origin of eukaryotic cellular complexity. *Nature*, *541*, 353–358.

Zhang, F., Bian, J., Chen, X., Huang, J., Smith, N., Lu, W. et al. (2019) Roles for intracellular cation transporters in respiratory growth of yeast. *Metallomics*, *11*, 1667–1678.

Zíková, A., Verner, Z., Nenarokova, A., Michels, P.A.M. & Lukeš, J. (2017) A paradigm shift: the mitoproteomes of procyclic and bloodstream *Trypanosoma brucei* are comparably complex. *PLoS Pathogens*, *13*, e1006679.

SUPPORTING INFORMATION

Additional supporting information can be found online in the Supporting Information section at the end of this article.

How to cite this article: Wenger, C., Harsman, A., Niemann, M., Oeljeklaus, S., von Känel, C., Calderaro, S., Warscheid, B. & Schneider, A. (2023). The Mba1 homologue of *Trypanosoma brucei* is involved in the biogenesis of oxidative phosphorylation complexes. *Molecular Microbiology*, *119*, 537–550. https://doi.org/10.1111/mmi.15048